Comparison of bonding and charge density in δ-UO_3, γ-UO_3, and La_6UO_{12}

L. Casillas-Trujillo,[1] G. Baldinozzi,[2] M. K. Patel,[3] H. Xu,[1] and K. E. Sickafus[1,*]

[1]*Department of Materials Science and Engineering, University of Tennessee, Knoxville, Tennessee 37996, USA*

[2]*Laboratoire Structures, Propriétés et Modélisation des Solides, Centre National de la Recherche Scientifique, Centralesupélec, 91190 Gif-sur-Yvette, France and Commissariat à l'Energie Atomique, DMN, SRMA, 91190 Gif-sur-Yvette, France*

[3]*Department of Mechanical, Materials, and Aerospace Engineering, University of Liverpool, Brownlow Hill, Liverpool L69 3GH, England, United Kingdom*

(Received 2 June 2017; published 16 November 2017)

This computational paper examines the effect of local atomic environments on the electron charge density in δ-UO_3, γ-UO_3, and La_6UO_{12}. In particular, this paper reveals differences in the uranium local atomic environments in these model oxide compounds. To examine the differences in a quantitative way, atoms-in-molecule (AIM) and Bader analysis methods were used to interrogate the electron charge density. The electron charge-density distribution in each compound was obtained using density functional theory. The AIM-Bader analyses provided estimates for the so-called Bader charges on individual lattice atoms, as well as the locations of the bond critical points (BCPs) between bonding atoms and the charge densities at the BCPs. Calculation results revealed a quantitative inverse correlation between the charge density at the BCP and the U-O bond length. In addition, this inverse correlation was found to be surprisingly similar to a well-established crystal chemical relationship between bond strength and bond length.

DOI: 10.1103/PhysRevMaterials.1.065404

I. INTRODUCTION

Complex uranium oxide atomic structures are formed during the life cycle of uranium dioxide (UO_2) nuclear fuel [1]. Fission products, especially lanthanide species, are incorporated into the UO_2 matrix as the fuel ages. One suspects that the stability and durability of the fuel may be influenced by local atomic arrangements in the vicinity of individual U atoms in the fuel. First-principles computational methods offer a means to interrogate such local atomic environments in complex materials, and in particular to determine the equilibrium electron charge density. In this context, it is possible to analyze the calculated electron charge density using so-called atoms-in-molecule (AIM) methods [2], in an effort to gain additional "chemical" insight, such as bonding ionicity or covalency. Such information may help us to better understand atomic structural stability and even, perhaps, to predict material stability in extreme environment applications such as nuclear energy production.

AIM analyses are commonly employed in chemistry to study charge distribution in molecules, but AIM has also been used to examine electronic charge distributions in crystalline solids. Many AIM-related studies have been performed on a wide variety of materials such as cuprates [3], beryl [4], spodumene [5], lithium-based compounds [6–10], silicates [11,12], and oxides [13]. For compounds incorporating heavy elements such as lanthanides and actinides, assessment of the charge density via experiments is often difficult. Thus, computational simulation is an attractive alternative. In particular, density functional theory (DFT) is capable of obtaining the electron charge densities of compounds containing heavy elements. AIM analyses (and related Bader analysis procedures) in the form of the charge basin integration have been performed on heavy element bearing oxides such as UO_2 [14,15] and $Ln_2Tc_2O_7$ [16] (where *Ln* stands for a lanthanide species), but to date no study has analyzed the characteristics of the charge density at the critical points.

In this paper, we use the AIM-Bader approach, hereafter abbreviated AIM-B, to analyze quantitatively specific features of the electron charge density in three model uranium (U) bearing oxide compounds: (i) δ-UO_3, (ii) γ-UO_3, and (iii) La_6UO_{12}. These compounds are related in the sense that U atoms in each compound have a "formal" valence of 6+ and possess a closed-shell electronic configuration. We first obtain the electron charge-density distributions using DFT. With this, we calculate the Bader charges and obtain the nature of the bonds via analyses of the principal curvatures of the charge density at the bond critical points (BCPs), as well as the Laplacian magnitude at these bond critical points.

II. STRUCTURAL MODELS

δ-UO_3 possesses a cubic ReO_3-type crystal structure with one formula unit per unit cell. δ-UO_3 belongs to space group $Pm\bar{3}m$ (S.G. no. 221), with a U atom at Wyckoff equipoint 1*a* and an O atom at Wyckoff equipoint 3*d* [17]. In this structure, the fundamental coordination polyhedron associated with each U atom is a regular octahedron with 2.097-Å nearest-neighbor (NN) U-O bond distances and 90° O-U-O bond angles (calculation results, this paper). The crystal structure of δ-UO_3 is shown in Fig. 1. All octahedra are corner sharing in δ-UO_3.

γ-UO_3 is the most thermodynamically stable polymorph of UO_3 [18], and it is the most complicated crystal structure among the compounds in this paper. γ-UO_3 possesses an orthorhombic crystal structure and belongs to space group *Fddd* (S.G. no. 70). In this paper, we use the standardized crystal structure convention, such that the structure of γ-UO_3 is described in the second setting of space group *Fddd*, such that the unit-cell origin is on a center of symmetry (point symmetry $\bar{1}$) at Wyckoff special equipoint 16*c*. The γ-UO_3

*Corresponding author: kurt@utk.edu

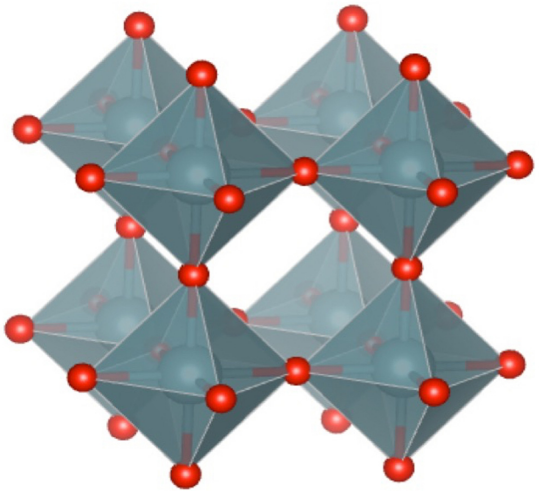

FIG. 1. Crystal structure of δ-UO_3. Oxygen atoms (shown in red) occupy the vertices of regular octahedra that constitute the nearest-neighbor polyhedra of uranium atoms. Each octahedron contains a uranium (light-colored sphere) at its center. The cube formed by linking the U atoms in the diagram is the unit cell of δ-UO_3.

orthorhombic unit cell contains 32 formula units. Figure 2 shows the crystal structure of γ-UO_3. There are two distinct U sites: U1 at Wyckoff special equipoint 16*g* and U2 at equipoint 16*c* on the unit-cell origin. There are three distinct O sites, all utilizing the general Wyckoff equipoint, 32*h*, but with different fractional coordinate definitions [19]. U1 atoms are bonded to

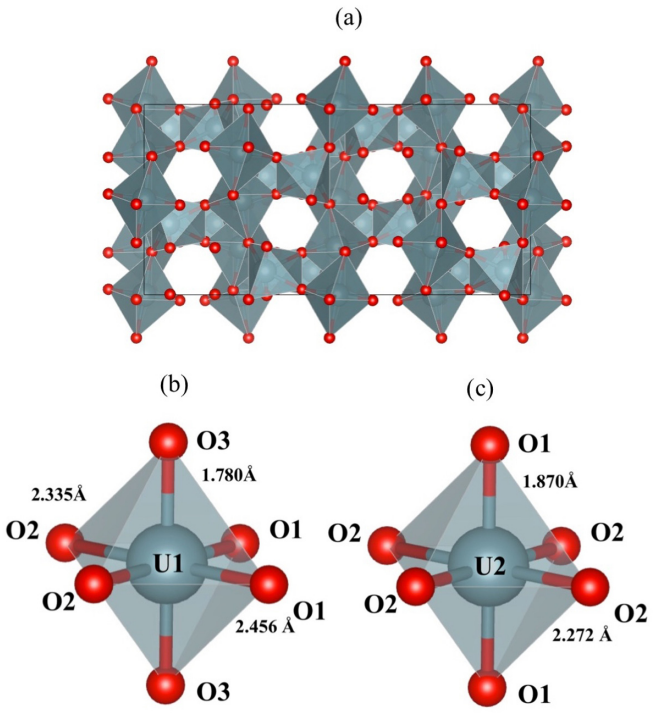

FIG. 2. (a) Projection of the orthorhombic unit cell of γ-UO_3, viewed along the *c* axis (O coordination polyhedra are shown around central U atoms). (b) Nearest-neighbor coordination polyhedron for U1 atoms. (c) Nearest-neighbor polyhedron for U2 atoms. The numerical bond lengths shown in (b) and (c) are based on calculation results from this paper.

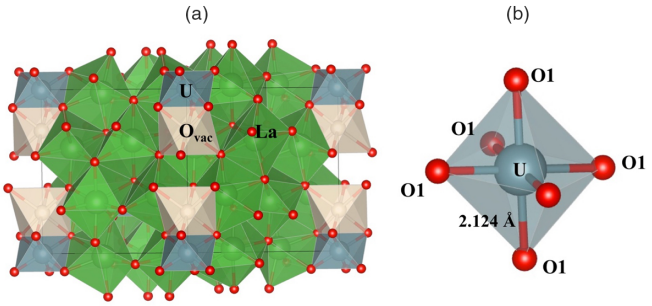

FIG. 3. (a) Crystal structure of La_6UO_{12}. O atoms in red form the vertices of the coordination polyhedra. The translucent green polyhedra are the coordination polyhedra for La atoms; the translucent dark blue/gray distorted octahedra correspond to U atoms. White octahedral cages highlight the environment of the vacant sites in the oxygen sublattice. (b) Coordination polyhedron for a U atom in La_6UO_{12}. O atoms in red occupy the vertices of the irregular octahedron. The numerical bond length shown in (b) is based on calculation results from this paper.

six nearest-neighbor O atoms, forming a distorted octahedron, having two O1, two O2, and two O3 bonds [Fig. 2(b)]. There are two other O3 atoms that might be considered as nearest neighbors to U1; however, these O3 atoms are located considerably farther away than all the other neighbors at 3.23 Å (calculation results, this paper).[1] U2 atoms are surrounded by six O nearest neighbors forming a distorted octahedron, and they are only bonded to O1 and O2 atoms [Fig. 2(c)]. U2 atoms are edge sharing with other U2 nearest-neighbor polyhedra and corner sharing with U1 polyhedra. It is also important to note that in γ-UO_3 the U1-O3 and U2-O1 bonds are short in a *uranyl* (O-U-O molecular unit) manner.

La_6UO_{12}, commonly referred to as the δ phase in the literature, possesses a fluorite derivative structure and should not be confused with the δ polymorph of UO_3. This structure is typically described using a hexagonal unit cell. The La_6UO_{12} structure belongs to space group $R\bar{3}$ (S.G. no. 148) [20] with U and La atoms at the 3*a* and 18*f* Wyckoff equipoints, respectively. There are two distinct O sites, O1 and O2, in the La_6UO_{12} structure, both located on 18*f* Wyckoff equipoints, but with different fractional coordinate definitions. Also, the structure can be thought of as containing oxygen vacancies located at the 6*c* Wyckoff equipoint. The O vacancies are close to the U atoms in such a way that the U coordination number is 6 forming an octahedron. Octahedral coordination polyhedra are typical for U^{6+} ions in ionic solids. In La_6UO_{12}, U atoms only have O1-type atoms as nearest neighbors. The coordination octahedron is close to a trigonal antiprism, with U-O1 bond distance of 2.124 Å and 83.88° O1-U-O1 angle (calculation results, this paper), instead of the 90° angle associated with a regular octahedron. La has seven nearest-neighbor O atoms, being bonded to both O1 and O2 atom types. The crystal structure of La_6UO_{12} is shown in Fig. 3.

[1]Some authors include next-nearest-neighbor O3 anions in their descriptions of coordination polyhedra associated with U1 cations in γ-UO_3. When including these extra two O3 anions, the coordination polyhedron for U1 is described as a bicapped trigonal prism.

III. COMPUTATIONAL METHODS

A. DFT calculations

DFT calculations were performed to obtain the electron charge densities in the model uranium oxide compounds of interest in this paper. For these calculations, we used the generalized gradient approximation exchange-correlation functional due to Perdew-Burke-Ernzerhof (PBE) [21]. The uranium $6s^2\ 6p^6\ 5f^3\ 6d^1\ 7s^2$, the lanthanum $5s^2\ 5p^6\ 5d^1\ 6s^2$, and the oxygen $2s^2\ 2p^4$ electrons are treated as valence electrons. The electron-ion interaction is described by the projector augmented wave method [22], and the plane-wave basis energy cutoff was set to 500 eV. The Vienna *ab initio* package VASP [23,24] was employed to perform the simulations. We used a $4 \times 4 \times 4$ k-point sampling grid.

To account for the strongly correlated f electrons, we employed the Hubbard $+U$ correction in the rotationally invariant Dudarev formulation [25], with parameters for U and J of 4.5 and 0.51 eV, respectively. These parameters were originally derived by Dudarev *et al.* [26], based on experimental measurements on UO_2. We have used these values since there were no parameters available that relate specifically to our U-bearing model compounds, and they have been used previously for diverse uranium compounds including UO_3 polymorphs and provide the correct band gap of these materials [27,28]. Nevertheless, we performed a complete assessment on the dependence of the charge-density quantities on the choice of the $+U$ parameters for the δ-UO_3 polymorph.

In all VASP computations, the atomic positions and shape of the structures were relaxed until the magnitude of the forces was below 10^{-2} eV/Å or until the internal energy converged to at least 10^{-5} eV.

B. AIM analysis

While electron density is readily obtained from DFT simulations, the charge on a given ion is not so similarly evident, as it depends on the choice of model or theory to partition the electron density between atomic centers. There is no unambiguous means to perform the partitioning because the wave functions of electrons in the crystal are multicentered and delocalized, as required by quantum mechanics. Using the framework of the atoms-in-molecules theory proposed by Bader [2], atoms are defined through a partitioning of real space, and the gradient of the electron density is used to define where one atom basin ends and the next begins. AIM theory provides a quantitative way to analyze the topology of the charge density, ρ, by means of its first derivative, $\nabla(\rho)$. At the critical points, this gradient vanishes. The characteristics of these points are determined by the Hessian of ρ. In extended solids, the Hessian is the (3×3) real and symmetric matrix of partial second derivatives. At a critical point, the eigenvalues of the Hessian are all real. The critical points are distinguished by their rank and signature. The rank is defined as the number of nonzero eigenvalues, while the signature is defined as the algebraic sum of the signs of the eigenvalues. For topologically stable critical points, the rank is always 3. The four possible critical points are (1) the nuclear critical point $(3, -3)$ with all curvatures negative, e.g., a local maximum that corresponds to an atom nucleus; (2) the bond critical point $(3, -1)$ where two curvatures are negative and one is positive, and a saddle point corresponds to interatomic bonding; (3) the ring critical point $(3, +1)$ where two curvatures are positive and one is negative; and (4) the cage critical point $(3, +3)$ where all curvatures are positive, which is indicative of a local minimum in the electron charge density. Associated with each critical point is a set of trajectories of $\nabla(\rho)$ that start at the critical point and terminate at another critical point (or at infinity in a molecule). They define a zero-flux interatomic surface, a surface that encloses each atom, resulting in a unique means of partitioning the crystal into separated atomic basins. Those surfaces are usually very far from spherical in shape (the shape usually associated with an atom). The volume of each basin can be measured. Moreover, by integrating the electronic density within those basins where an atom nucleus is located, the total charge on an atom can be obtained. The lines of maximum charge density linking the nuclei of two atoms are called bond paths. The bond path crosses the surface of the basins at the BCP. The shape of the electron density at a BCP has a saddle shape, therefore the two eigenvalues λ_1 and λ_2 of the matrix along axes normal to the bond path are positive while the eigenvalue λ_3 along the internuclear axis of the bond is negative.

The critical point searches were performed using the AIM-UC software developed by Vega and Almeida from the University of Carabobo [29], while charge basin integrations were performed using the Bader software developed by the Henkelman group at the University of Texas [30].

IV. RESULTS

Table I provides the crystal structure parameters obtained by DFT calculations for the compounds of interest in this paper. For comparison, similar structural parameters from selected experimental studies are also shown in Table I.

Next, we introduce the results of our AIM-B analyses by considering the electron charge-density distribution in the compound with the highest crystallographic symmetry of those we examined in this paper, namely, the δ-UO_3 phase. Figure 4 shows a contour map of the electron charge density for δ-UO_3 in a $\{001\}$-type plane. In Fig. 4, the U atom occupies the center and it is surrounded by four O NN. The other two O nearest neighbors lie above and below the U atom (out of the plane of the drawing). The electron density is higher close to the nuclear Bader critical point, and it decreases as the distance from the nuclear critical point increases. The BCPs are located in between the nuclear critical points.

Table II summarizes the U-O bond lengths for the different compounds examined in this paper, and the position of the BCP with respect to the U and O atoms. Table III shows the partial charges along with the associated atomic volumes for U and O in δ-UO_3, γ-UO_3, and La_6UO_{12}. The partial charge values ($\tilde{\delta}$) in Table III represent the numbers of electrons each atom loses or gains upon bonding. These values are obtained by the integration of charge in the atomic basins. Note that loss of electrons results in a plus sign for partial charge, while gain of electrons yields a minus sign (as is the convention for describing cations and anions, respectively). Table IV provides the following properties of the BCPs for the U-O bonds in the same compounds: the Hessian eigenvalues λ_i,[2] the charge

[2]The Hessian eigenvalues λ_i represent the principal curvatures of the charge density at the bond critical point (ρ_{BCP}).

TABLE I. Lattice parameters and related crystal structure data for relaxed structures of δ-UO_3, γ-UO_3, and La_6UO_{12}, obtained via DFT calculations. Selected experimental data are also shown for comparison to the DFT results.

Method	a (Å)	b (Å)	c (Å)	Volume/formula unit (Å^3/f.u.)	Average volume/atom $\langle\Omega_a\rangle$ (Å^3/atom)
			δ-UO_3 (cubic)		
PBE + U	4.194	4.194	4.194	73.77	18.44
Expt. [17]	4.165	4.165	4.165	72.25	18.06
			γ-UO_3 (orthorhombic)[a]		
PBE + U	9.937	9.932	20.736	63.95	15.99
Expt. [19]	9.711	9.813	19.930	59.35	14.84
			La_6UO_{12} (hexagonal)		
PBE + U	10.526		10.037	321.03	16.88
Expt. [20]	10.468		9.982	315.76	16.62

[a]The orthorhombic γ-UO_3 data shown here are in the *standardized* crystal structure data format, rather than the *published* crystal structure data format. In standardized form, the origin of the unit cell is at a center of symmetry ($\bar{1}$) and the orthorhombic lattice parameters are arranged such that $c > b > a$.

density at the BCP ρ_{BCP}, the Laplacian, the curvature ratio $|\lambda_1|/\lambda_3$, and the ellipticity.

V. DISCUSSION

A. DFT simulation results on crystal structures of model U-bearing oxides

The DFT calculated crystal structure results shown in Table I are in good agreement with the reported experimental results [17,19,20], differing at most by 4%. It should be noted that for all compounds investigated here DFT finds a larger unit-cell volume than experiment. Our δ and γ-UO_3 results are also in good agreement with published results from previous computational studies of UO_3 polymorphs [27,28,31,32]. It should be noted that the γ-UO_3 structure has the highest atomic density of the compounds examined in this paper, while the δ-UO_3 polymorph is the least dense. The higher density of γ-UO_3 compared to δ-UO_3 is largely attributable to a mixture of both edge- and corner-shared octahedra in the γ phase, versus only corner-shared octahedra in the δ phase (edge sharing leads to a higher packing density).

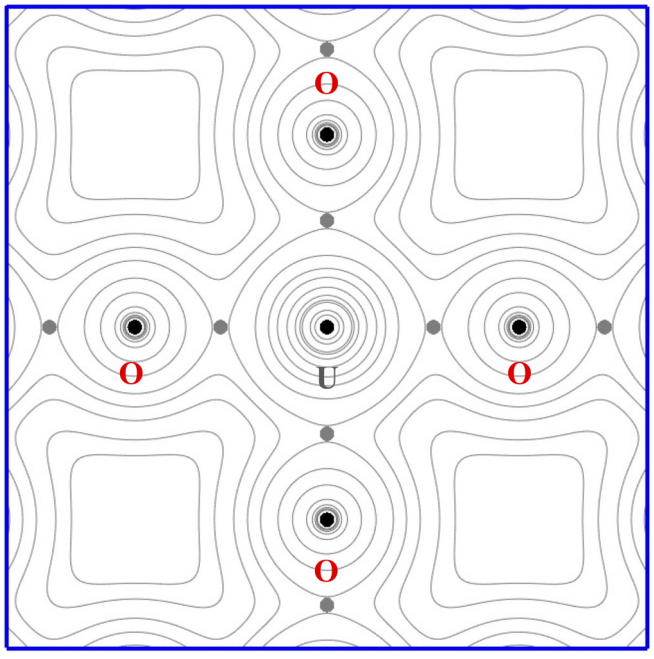

FIG. 4. Contour map of the calculated electron charge density for δ-UO_3 in a {001}-type plane. Nuclear U and O critical points are shown as black dots, while the BCPs are shown as gray dots.

B. Coordination polyhedral unit for U1 in γ-UO_3

The U1 nearest-neighbor polyhedron in γ-UO_3 is commonly presented in the literature as a complex polyhedral unit consisting of eight nearest-neighbor anions: two O1-, two O2-, and four O3-type atoms [27], with two of the O3 atoms located considerably more distant from the U1 central atom at 3.24 Å (number from this paper), compared to the

TABLE II. Calculated U-O bond lengths and BCP positions in δ-UO_3, γ-UO_3, and La_6UO_{12}. Also shown are the percentages of the U-O bond lengths that are assignable to the U and O ions, based on the position of the BCP.

	Bond length (Å)	BCP distance to U (Å)	BCP distance to O (Å)	U bond %	O bond %
			δ-UO_3		
U-O	2.097	1.163	0.934	55.46	44.54
			γ-UO_3		
U1-O1	2.456	1.363	1.093	55.50	44.50
U1-O2	2.335	1.282	1.054	54.88	45.12
U1-O3[a]	1.780	0.986	0.794	55.40	44.60
U2-O1	1.870	1.033	0.837	55.24	44.76
U2-O2	2.272	1.249	1.023	54.97	45.03
			La_6UO_{12}		
U-O1	2.124	1.179	0.945	55.50	44.50

[a]The U1-O3 bond shown here is the "uranyl-like" nearest-neighbor bond. The much longer next-nearest-neighbor U1-O3 bond is not shown in this table, but is discussed in the text (Sec. II) and included in the data shown in Fig. 6.

TABLE III. Calculated partial charge, $\tilde{\delta}$, and atomic volume, Ω_a, for U and O in δ-UO_3, γ-UO_3, and La_6UO_{12}, based on AIM-B analysis. Also shown are the partial charge and atomic volume for La in La_6UO_{12}. The γ-UO_3 compound is characterized by two distinct U atom positions and three O positions.

	Partial charge/atom $\tilde{\delta}$ (eV/atom)	Volume/atom Ω_a (Å^3/atom)
	δ-UO_3	
U	+3.09	15.568
O	−1.03	19.403
	γ-UO_3	
U1	+2.92	15.49
U2	+2.91	16.47
O1	−0.94	15.61
O2	−1.16	14.77
O3	−0.81	17.57
	La_6UO_{12}	
U	+2.88	15.52
La	+2.06	19.47
O1	−1.21	15.74
O2	−1.33	15.71

other six O anions. In Fig. 2 and Table II, we present the nearest-neighbor polyhedron for the U1 atom as a distorted octahedron, with six nearest-neighbor atoms. In our AIM-B analysis, we did not find a BCP between U1 and the longer-distance O3 atoms, indicating that bonding between these atoms is inconsequential. This is the reason we describe bonding to U1 using an octahedral nearest-neighbor anion polyhedron representation.

C. Experimental versus theoretical crystal structures of La_6UO_{12}

Table I indicates that for La_6UO_{12} the calculated average atomic volume, $\langle\Omega_a\rangle$, is about 1.5% larger than the experimental value. In contrast, the calculated volume of the U octahedral coordination polyhedron in La_6UO_{12} (i.e., the volume inscribed by nearest-neighbor O anions surrounding a central U cation) is about 4.3% smaller than the experimental volume (12.55 versus 13.12 Å^3). This paradox is resolved when we consider the La coordination polyhedra in La_6UO_{12}. We find a larger La coordination polyhedron using DFT than is found in experiments (22.87 versus 21.94 Å^3). Since La ions are much more numerous than U ions in La_6UO_{12}, this explains why we find a larger $\langle\Omega_a\rangle$ for La_6UO_{12} using DFT compared to experiment.

D. AIM-B atomic radii versus classical ionic radii in δ-UO_3

Next, it is instructive to compare and contrast atomic radii obtained via AIM-B analysis (based on the locations of the BCPs) versus the Shannon [33] ionic radii. For this comparison, we consider our *benchmark* compound, δ-UO_3, which has the highest symmetry of the model compounds we have considered in this paper. Figure 5 shows the gradient vector field of the electron charge density surrounding a central U atom in a {001}-type plane of δ-UO_3. The drawing in Fig. 5 includes both the nuclear critical points for the central U atom and the nearest-neighbor O atoms, as well as the BCP positions between the central U and surrounding O atoms. In Fig. 5, we have overlaid shaded circles on the gradient vector field plot, which are intended to represent U and O ions with ionic radii corresponding to their "formal" valences of 6+ and 2−, respectively. These radii are based on Shannon [33] and correspond to sixfold coordination of U atoms by nearest-neighbor O, and twofold coordination of O atoms by nearest-neighbor U. The Shannon radius for a sixfold coordinated U^{6+} ion is 0.73 Å, while the radius for a twofold coordinated O^{2-} ion is 1.35 Å, giving a U-O bond length of 2.08 Å. The BCP in the AIM-B approach is located 1.163 Å from the U nucleus and 0.934 Å from the O nucleus. This leads to a U-O bond length of 2.097 Å, which is only 0.8% larger than the U-O bond length obtained using Shannon radii. The BCP position differs from the Shannon dividing point between adjacent U and O ions, being closer to O with AIM-B. The locations of the BCPs along with the gradient field of the electron charge density serve to define the atomic basins. The shape of the atoms in the AIM-B approach differs greatly from the spherical ionic picture. One difference between the AIM-B and ionic atom descriptions arises from Shannon's underestimation of the U ion size, which is based on its formal valence of 6+ (and

TABLE IV. BCP characteristics for U-O bonds in δ-UO_3, γ-UO_3, and La_6UO_{12}, based on AIM-B analysis. Note that O2 in La_6UO_{12} does not bond to U.

	Hessian eigenvalues			Charge density		Curvature	
Bond	λ_1	λ_2	λ_3	ρ_{BCP} (eV/Å^3)	Laplacian	Ratio $\lvert\lambda_1\rvert/\lambda_3$	Ellipticity
				δ-UO_3			
U-O	−4.557	−4.557	17.669	0.928	+8.555	+0.258	0
				γ-UO_3			
U1-O1	−1.732	−1.546	7.933	0.395	+4.654	+0.218	0.120
U1-O2	−2.165	−2.101	9.829	0.526	+5.564	+0.220	0.030
U1-O3[a]	−14.564	−14.268	33.040	2.141	+4.208	+0.441	0.021
U2-O1	−10.346	−10.317	28.065	1.685	+7.402	+0.369	0.003
U2-O2	−2.800	−2.608	12.273	0.644	+6.863	+0.228	0.074
				La_6UO_{12}			
U-O1	−4.912	−4.296	15.284	0.906	+6.076	+0.321	0.236

[a]The U1-O3 bond shown here is the "uranyl-like" nearest-neighbor bond length.

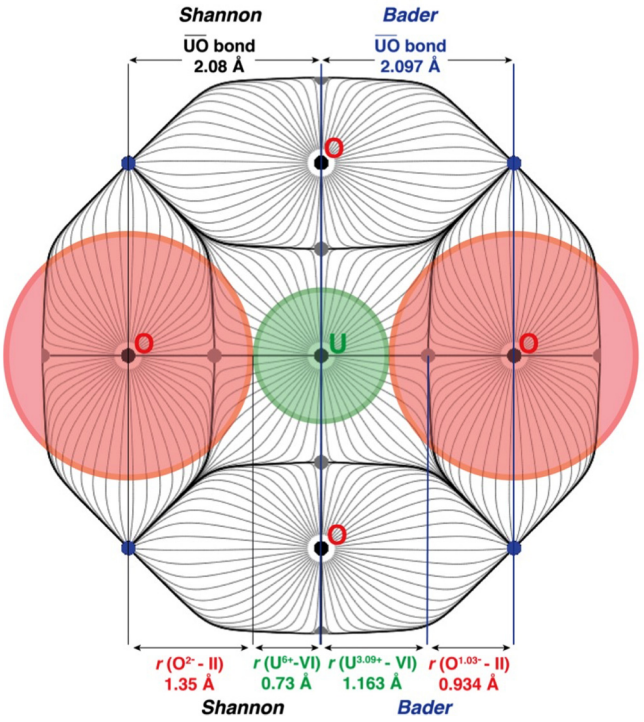

FIG. 5. Gradient vector field associated with the calculated electron charge density for δ-UO_3 in a $\{001\}$-type plane. The shaded circles represent ion sizes in the Shannon "formal" valence approach. The position of the AIM-B BCP for the U-O bond on the right is delineated by a blue line. The Shannon bonding point for the O-U bond on the left is delineated by a thin black line.

corresponding overestimate of the O ion size, which is based on its formal valence of 2−). A U^{6+} cation is very small due to its lack of outer valence electrons. The larger U ion from AIM-B analysis can be rationalized using Sanderson's principle of electronegativity equalization [34]. According to Sanderson, charge transfer occurs while there are differences in electronegativity, but as the transfer progresses the electronegativities of both elements become more similar. By consequence, charge transfer ceases long before the U and O ions achieve their formal valences of 6+ and 2− respectively.

E. BCP positions between bonding U and O ions

From Table II, we find that in all cases the BCP is not located at the midpoint of the bonding distance, but rather resides closer to the O atoms. We have quantified how much of the bond length "belongs" to each atom. For all compounds, we found that ∼55% of each U-O bond belongs to the U atom, versus ∼45% belonging to the oxygen atom (Table II). We are comparing U-O bonds in our model compounds; consequently, in Table II we did not include data for La-O bonds in La_6UO_{12}. The La-O bond length in La_6UO_{12} is nondegenerate, with a rather short average La-O2 bond length of 2.41 Å versus a longer average La-O1 bond length of 2.65 Å. It should be noted that O2 anions are bonded only to La cations, while O1 anions are bonded to U and La cations.

F. Partial charges on constituent U and O ions

Next, our AIM-B analyses reveal that charge transfer from U cations to neighboring O anions (or vice versa) in the model oxides examined here is dependent on crystal structure and chemical environment. For compounds investigated in this paper, all the charge is transferred from the cations to the anions and no charge is trapped in interstitial positions. In δ-UO_3, each U atom loses ∼3.1 electrons, and the charge is evenly distributed among the neighboring O atoms. For γ-UO_3, both U1 and U2 positions have a similar net charge, each U having transferred ∼2.9 electrons to neighboring O atoms. This transferred charge is not evenly distributed with respect to the surrounding O anions, as was the case for δ-UO_3; instead, each type of O atom receives a different amount of charge. In the case of La_6UO_{12}, the U atoms transfer ∼2.9 electrons to neighboring O1 atoms. We also identified differences in charge transfer to O1- and O2-type atoms in La_6UO_{12}. The O atoms that are bonded to both U and La atoms (labeled O1 in Table III) receive less charge than the O atoms that are only bonded to La atoms (labeled O2). The U atom transfers less charge to O compared to the UO_3 polymorph cases while, in contrast, the O atoms receive more charge than for the UO_3 polymorph cases. This apparent paradox is resolved when one considers that the coordination of O is higher in La_6UO_{12} than in UO_3 polymorphs (therefore more nearest-neighbor cations contribute charge to a given O anion). The charge-transfer values from U atoms to neighboring O atoms found in this paper (ranging from +2.88 to +3.09) are slightly greater than the values obtained in previously published computational studies of oxides containing uranium. In particular, in UO_2, the charge on U was found to be +2.6 electrons [15,35].

G. Bond ionicity versus bond covalency

Next, we address U-O bond ionicity, or its complement bond covalency, in our model compounds, based on application of Bader-Essen rules [36] to our AIM-B results. Certain characteristics of the BCPs are related to bond ionicity (or, conversely, to covalency). For instance, positive values of the Laplacian and positive curvature ratio at the BCP are indicators of closed-shell interactions, i.e., ionic bonding. Negative values of the Laplacian and the curvature ratio indicate shared interactions, i.e., covalent bonding. In our paper, all of the BCPs exhibit positive values for the Laplacian and the curvature ratio. Therefore, all bonds in our model compounds are dominated by closed-shell (ionic) interaction characteristics. However, we find evidence for variations in relative bond ionicity, since we observe variations in the magnitudes of the Laplacian and the curvature ratio among the U-O BCPs. The bond with the most covalent-like characteristics is the U1-O3 bond in γ-UO_3 (this is one of the *uranyl*-like bonds). This bond possesses the lowest Laplacian value and the highest value of the curvature ratio, compared to all U-O bonds evaluated in this paper (note that a small magnitude for the curvature ratio, namely, $|\lambda_1|/\lambda_3 \ll 1$, is indicative of closed-shell interactions [6]). It is also important to note that this U1-O3 bond in γ-UO_3 exhibits the largest charge at the BCP, ρ_{BCP}, of all BCPs examined. This charge, which is representative of shared charge between atomic constituents, is also indicative of more covalency in the bond. Our AIM-B analysis revealed a strong correlation between ρ_{BCP} and the BCP curvature ratio, namely, the greater the BCP curvature ratio the greater the value of ρ_{BCP}.

H. Charge densities at the U-O BCPs versus bond lengths and bond strengths

The most notable finding in our paper is a definitive inverse (negative) correlation between the U-O bond length, r_{UO}, and the charge density at the BCP, ρ_{BCP}. We find that the shortest U-O bonds possess the largest ρ_{BCP} values, and vice versa (Tables II and IV). We discovered that there is a quantitative trend in ρ_{BCP} versus r_{UO}, and this trend incorporates all of the compounds that we investigated. Our ρ_{BCP} versus r_{UO} data can be fit to an exponential function with rather high precision. Specifically, we find

$$\rho_{BCP} = \rho_0\, e^{\frac{r_0 - r}{B}} = e^{\frac{2.0822 - r}{0.4004}} \quad \left[\frac{\text{eV}}{\text{Å}^3}\right], \quad \chi^2 = 0.00345,$$
$$r_0 = 2.0822\,[\text{Å}], \quad B = 0.4004\,[\text{Å}], \tag{1}$$

where ρ_{BCP} is the charge density at the BCP in units of eV/Å^3; ρ_0 is the value of ρ_{BCP} at $r = r_0$ and is arbitrarily set to $1\,\text{eV/Å}^3$; r is the U-O bond length (r_{UO}) in units of angstroms; r_0 and B are exponential fitting parameters, both in units of angstroms.[3] Equation (1) indicates that as the U-O bond length decreases the charge density at the BCP increases exponentially. This BCP charge is effectively the "shared" charge between the U and O ions participating in the bond. In other words, the BCP charge represents the covalent component of the mixed ionic-covalent bond, and this covalent bond component increases with decreasing bond length.

The exponential fitting function in Eq. (1) is the same form as a function used by Zachariasen [37] to relate a parameter called *bond strength* (s) to bond length (r) in oxygen and halogen compounds containing d and f electron metal cations. In fact, if we use a set of experimentally determined U-O bond lengths, r, in U^{6+}- and O^{2-}-bearing compounds (using the U and O formal valences) published by Zarchariasen (Table 1 in [38]), we can calculate a corresponding set of bond strengths, s, for these U-O bonds, based on the following exponential relationship between s and r due to Brown and Altermatt [39]:

$$s = s_0\, e^{\frac{r_0 - r}{B}} = e^{\frac{2.075 - r}{0.370}} \quad [\text{esu}],$$
$$r_0 = 2.075\,[\text{Å}], \quad B = 0.370\,[\text{Å}], \tag{2}$$

where s is the bond strength in electrostatic units (esu); s_0 is the value of s at $r = r_0$ and is arbitrarily set to 1 esu; r is the U-O bond length (r_{UO}) in units of angstroms; and r_0 and B are constants, both in units of angstroms. We note that the fitting constants r_0 and B in Eq. (2) are very similar to the corresponding constants in Eq. (1). In Fig. 6, we overlay a comparison between our ρ_{BCP} versus r_{UO} computational results and the s versus r_{UO} values determined by the method summarized above. The plot in Fig. 6 employs reduced (dimensionless) units, namely, r/r_0 for the fractional U-O bond length, ρ_{BCP}/ρ_0 for the fractional BCP charge, and s/s_0 for the fractional bond strength [based on Eqs. (1) and (2)]. Figure 6 provides strong evidence for a direct correlation between the charge density, ρ_{BCP}, at the U-O BCP (determined via AIM-B analysis) and the U-O bond strength, s, as derived using a methodology similar to Zachariasen [37]. This relationship between ρ_{BCP} and bond strength was also identified by Gibbs *et al.* in DFT simulations of oxide and hydroxyacid molecules [40], and crystalline silicates and oxides [41].

To test the predictive capabilities of the ρ_{BCP}/ρ_0 versus r/r_0 curve shown in Fig. 6, we performed DFT calculations and an AIM-B analysis on another U-bearing complex oxide not originally selected for this paper, namely, $BaUO_4$. These results are also shown in Fig. 6. There are three distinct U-O bond lengths in $BaUO_4$ and the calculated charge densities at the BCPs for these different bonds result in data points that fall very nearly on the exponential fitting curve relating ρ_{BCP}/ρ_0 to r/r_0. This gives us confidence that we can predict ρ_{BCP} based on knowledge of specific U-O bond lengths (either measured or calculated), at least for compounds containing U cations nominally with valence 6+.

It is useful to speculate on reasons for the surprising correlation we have found between ρ_{BCP} and s. The bond strength methodology used by Zachariasen [37,38] was originally conceived by Pauling [42] and used to explain how oxidation of a central cation in a nominally ionic compound can progress to the extent that the cation achieves its formal ionic valence, through bonds involving *only* NN ligands. For example, consider δ-UO_3 wherein each U cation is coordinated by six NN O anions in *regular* octahedral coordination. Pauling's *bond valence sum* (BVS) method stipulates that, in order for a U cation to achieve its formal 6+ valence, each NN O anion must contribute a bond strength of 1 esu. Each O anion, on the other hand, has a formal valence of 2− and these two electron charge units are donated to the O anion by two adjacent NN U cations. This leads to a net strength of 1 valence unit that any given O anion can contribute to a bond with any particular neighboring U cation. Since there are 6 NN O anions to the central U cation, the net valence delivered to the U is $6 \times (1\,\text{esu}) = 6\,\text{esu}$. This satisfies the U cation formal valence requirement of U^{6+} in the trioxide, δ-UO_3.

However, most complex structures consist of irregular coordination polyhedra, not regular polyhedra (the latter being the case in δ-UO_3). The compounds γ-UO_3 and La_6UO_{12}, for example, are dominated by irregular coordination polyhedra. These irregular polyhedra often are accompanied by concomitant bond-length nondegeneracy. We infer from this bond-length nondegeneracy that all NN bonds can no longer be equal; some bonds must be stronger than others. Zachariasen [37] proposed that shorter bond lengths must correspond to larger bond strengths (Zachariasen also proposed a corollary to this rule, namely, that bonds of equivalent length have equivalent strength). Zachariasen also proposed that a bond-length–bond-strength inverse correlation is applicable to bonding in compounds of any bonding type, be it ionic, covalent, or mixed.[4] In addition to having general applicability, Zachariasen's bond-length–bond-strength relationship

[3] We note that a power-law functional (not shown here) provides a fit that has nearly identical precision to the exponential fit shown in Eq. (1). We use the exponential fit in this paper because it is easiest to compare to published studies relating bond strength and bond length (next discussion topic).

[4] This was a problem with Pauling's BVS model. Pauling assumed that atomic radii are constant, with radii dependent on the type of

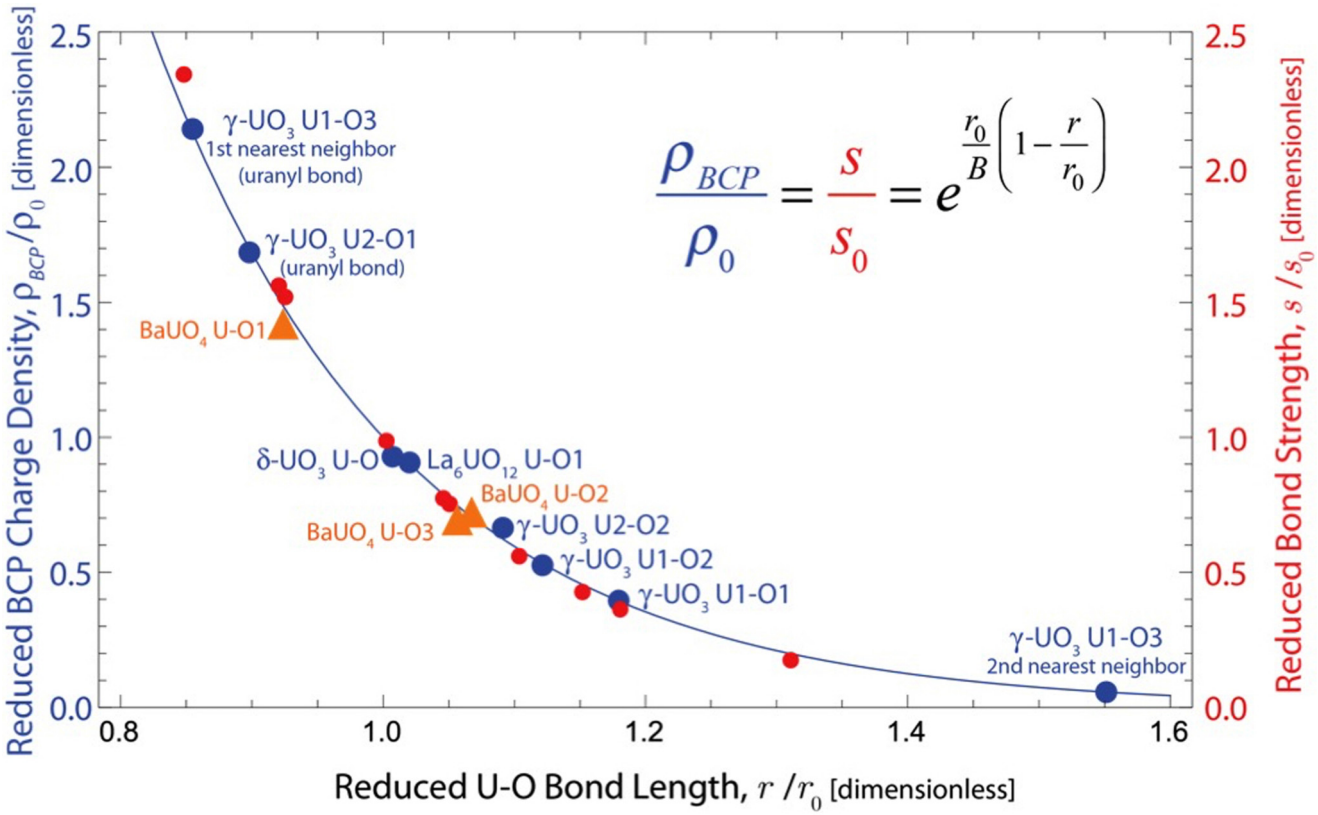

FIG. 6. Reduced charge density at the bond critical point (ρ_{BCP}/ρ_0) and reduced bond strength (s/s_0) vs reduced U-O bond length (r/r_0). The blue data points are from this paper and are labeled according to compound and particular U-O bond (these data points correspond to the left-hand ordinate in the plot). The bond lengths associated with the red data points are from Zachariasen [38] and represent a variety of U-bearing compounds containing nominally U^{6+} cations. The bond strengths associated with the red data points are calculated based on Eq. (2) from Brown and Altermatt [39] (these data points correspond to the right-hand ordinate in the plot). The solid blue line represents a fit to the blue data points, based on the fitting equation shown as an inset in the figure and using the fitting constants, r_0 and B, provided in Eq. (1) in the text. The fit to the red data points is not shown, but can be readily obtained from the same inset fitting equation, but using the r_0 and B fitting constants provided in Eq. (2) in the text. The triangular data points in orange are results of DFT calculations and AIM-B analysis on the U-bearing compound, $BaUO_4$ (this paper). These calculations were added to this study to test for possible universality of the correlation between ρ_{BCP} and s identified during the course of this paper. The value of the reduced BCP charge density for the γ-UO_3 U1-O3 next-nearest-neighbor bond data point in the plot was obtained using the reduced charge density associated with the blue fitting curve. In actuality, using AIM-B, we did not identify a BCP for this long next-nearest-neighbor bond.

has been further interpreted to suggest that shorter bonds are more covalent, while long bonds are ionic. In fact, Altermatt and Brown [43] attempted to quantify this notion, stating that "bonds with [strengths] greater than about 0.6 [esu] are those often described as covalent whereas weaker bonds correspond to those generally referred to as ionic or electrostatic." We believe that the quantitative inverse correlation between ρ_{BCP} and r_{UO} that we have identified in this paper, as well as the remarkably close relationship between the $\rho_{BCP}(r_{UO})$ and $s(r_{UO})$ dependences, provide direct evidence that stronger (i.e., shorter) heteroionic bonds are a result of increased bond covalency. In particular, this increased bond covalency is manifest in the increased shared electron charge that occurs in the vicinity of the BCPs that separate bonding atoms.

bonding (ionic or covalent). But in an irregular NN coordination polyhedron the radii of the ions that make up the polyhedron cannot all be the same.

I. Total BCP charge density versus partial ionic charge

In the last section, we concluded that increases in ρ_{BCP} affect corresponding increases in bond covalency. This leads us to postulate that increases in ρ_{BCP} should also be accompanied by concomitant decreases in charge transfer (i.e., decreased bond ionicity). To test this hypothesis on our model compounds, we endeavored to compare the total charge density residing at the BCPs adjacent to a central U cation to the partial charge, $\tilde{\delta}$, on this U cation, the latter derived via charge basin integration (Table III). We assume here that the total charge density at BCPs, ρ_{BCP}^{total}, can be represented by a sum of individual BCP charge densities for the U-O bonds associated with the nearest-neighbor O anions surrounding a central U cation. For instance, if we denote the BCP charge density of the ith nearest-neighbor O anion to the U cation as ρ_{BCP}^{i}, then ρ_{BCP}^{total} is given by $\rho_{BCP}^{total} = \sum_{i=1}^{i=N} \rho_{BCP}^{i}$, where N is the number of nearest-neighbor O anions to the central U cation. For all of the compounds we have investigated in this paper, $N = 6$

TABLE V. Total BCP charge density, ρ_{BCP}^{total}, based on a BCP charge density sum over nearest-neighbor anions surrounding a central U cation, and the integrated partial charge, $\tilde{\delta}$, for U atoms in δ-UO_3, γ-UO_3, and La_6UO_{12}, based on AIM-B analysis. The total BCP charge density is given by $\rho_{BCP}^{total} = \sum_{i=1}^{i=N} \rho_{BCP}^{i}$, where N is the number of nearest-neighbor O anions to the central U cation. The partial charge values in this table are the same as those in Table III. This table is arranged in order of increasing ρ_{BCP}^{total} for the U atoms in the various compounds.

	Total charge density, ρ_{BCP}^{total} (eV/Å^3)	Partial charge / U atom $\tilde{\delta}$ (eV/atom)
	La_6UO_{12}	
U	5.44	+2.88
	δ-UO_3	
U	5.57	+3.09
	γ-UO_3	
U2	5.95	+2.91
U1	6.12	+2.92

(U cations are in regular or distorted octahedral coordination with respect to nearest-neighbor O anions).

Table V shows a comparison between ρ_{BCP}^{total} and $\tilde{\delta}$ for U-O bonds in δ-UO_3, γ-UO_3, and La_6UO_{12}. This table is arranged in order of increasing ρ_{BCP}^{total} for the U atoms in the various compounds. Based on our hypothesis above, this implies that bond covalency should increase as one moves down the list of U cations in Table V. Conversely, we expected that bond ionicity, as indicated by the magnitude of the partial charge, $\tilde{\delta}$, should *decrease* moving down the list in the table. As is apparent from the data presented in Table V, this covalent-ionic inverse relationship that we postulated is not followed quantitatively. Considering only the binary oxides (δ-UO_3 and γ-UO_3) an inverse relationship between ρ_{BCP}^{total} and $\tilde{\delta}$ is nearly realized. However, inclusion of the ternary oxide, La_6UO_{12}, in the analysis does not lead to an inverse trend. There are likely several explanations for the failure of these results to support the complementarity between ionicity and covalency. For instance, in the ternary compound, La_6UO_{12}, the presence of neighboring La cations may be affecting charge transfer from the U cations to neighboring O anions. Also, in the γ-UO_3, we have not considered next-nearest-neighbor U-O interactions. However, these interactions may influence charge transfer from central U cations.

J. Testing the effects of variations in the Hubbard $+U$ correction on $\rho_{BCP}(r_{UO})$

The Hubbard parameters used in this paper (described in Sec. III A) yield calculated band gaps for our model compounds similar to those found in experiments. Specifically, our Hubbard parameters, $U = 4.5$ and $J = 0.51$, give band gaps of 2.19 and 2.35 eV for δ-UO_3 and γ-UO_3, respectively. These are in good agreement with reported experimental values, such as 2.17 eV for δ-UO_3 [44] and 2.38 eV for γ-UO_3 [28]. Nevertheless, we were unsure of the influence that Hubbard parameters might have on ρ_{BCP} values obtained from AIM-B analyses. To test this, we performed DFT simulations and AIM-B analyses in the model compound, δ-UO_3, wherein we varied the Hubbard $+U$ difference parameter, U-J, from zero to four, with zero corresponding to *standard* DFT (the specific values of U-J we used were zero, one, two, three, and four). First, we found that DFT overestimates the cubic lattice parameter, a, for δ-UO_3, regardless of the choice of U-J [45]. It should be noted that the equilibrium U-O bond length in δ-UO_3 scales in proportion to a ($r_{UO} = a/2$). Second, we found that the calculated band gap for δ-UO_3 increases in accordance with increasing U-J [45]. Third, we found that, irrespective of the value of U-J, the BCP position between bonding U and O ions exhibited the same partitioning as discussed in Sec. V E, namely, ~55% of the bond belongs to U and 45% belongs to O. Lastly, we found very small variations in ρ_{BCP} values as a function of U-J variation. Importantly, all of our newly calculated $\rho_{BCP}(r_{UO})$ values for varying U-J lie very nearly on our reduced charge density (ρ_{BCP}/ρ_0) versus reduced U-O bond-length (r/r_0) fitting curve (see Fig. 6 and [46]).

VI. CONCLUSIONS

In this paper, we used DFT and AIM-Bader analysis procedures to determine the electron charge-density distributions in three model uranium-bearing compounds: δ-UO_3, γ-UO_3, and La_6UO_{12}. We identified the BCPs between adjacent U-O atoms and we performed charge basin integrations in the AIM-Bader framework. We discovered that there exists a close relationship between the electron charge density at the BCP, ρ_{BCP}, and the bond strength, s, where s is a bonding property originally proposed by Pauling [42] and later refined by Zachariasen [37,38] and others. This relationship appears to be quantitative for compounds containing U-O bonds (work is in progress to test compounds containing metal constituents other than U). Our results suggest that using AIM-Bader methods we can determine the relative covalent bonding component of each bond in an irregular coordination polyhedron, based on the bond lengths of each bond to the central atom in this polyhedron. The covalency referred to here is the magnitude of the charge density at the BCP, and this magnitude is indicative of the degree to which electron charge is shared between bonding atoms. We believe that the results of this paper are directly applicable to other U-bearing compounds, in the sense that if we know U-O bond lengths for a given compound (based on crystal structure determination) we can immediately predict ρ_{BCP} for each U-O bond and assess relative covalency differences for all U-O bonds in the structure. We have already confirmed this prediction for one compound, namely, $BaUO_4$ (DFT results shown in Fig. 6).

ACKNOWLEDGMENTS

This work was performed under Grant No. DE-NA0001983 from the Stewardship Science Academic Alliances of the U.S. Department of Energy National Nuclear Security Administration. Computational simulations were performed using resources from the Newton High Performance Computing program at the University of Tennessee.

[1] D. A. Andersson, J. Lezama, B. P. Uberuaga, C. Deo, and S. D. Conradson, Cooperativity among defect sites in AO_{2+x} and A_4O_9 (A = U, Np, Pu): Density functional calculations, Phys. Rev. B **79**, 024110 (2009).

[2] R. F. Bader, *Atoms in Molecules* (John Wiley & Sons, Ltd., Hoboken, 1990).

[3] T. Lippmann and J. R. Schneider, Topological analyses of cuprite, Cu_2O, using high-energy synchrotron-radiation data, Acta Crystallogr. Sect. A **56**, 575 (2000).

[4] M. Prencipe, Ab initio Hartree-Fock study and charge density analysis of beryl ($Al_4Be_6Si_{12}O_{36}$), Phys. Chem. Minerals **29**, 552 (2002).

[5] M. Prencipe, M. Tribaudino, and F. Nestola, Charge-density analysis of spodumene ($LiAlSi_2O_6$), from ab initio Hartree-Fock calculations, Phys. Chem. Miner. **30**, 606 (2003).

[6] C. Gatti, Chemical bonding in crystals: New directions, Z. Kristallogr. **220**, 399 (2005).

[7] C. Gatti, P. Fantucci, and G. Pacchioni, Charge density topological study of bonding in lithium clusters, Theor. Chim. Acta **72**, 433 (1987).

[8] V. Luaña, A. Costales, and A. M. Pendás, Ions in crystals: The topology of the electron density in ionic materials. II. The cubic alkali halide perovskites, Phys. Rev. B **55**, 4285 (1997).

[9] A. M. Pendás, A. Costales, and V. Luaña, Ions in crystals: The topology of the electron density in ionic materials. I. Fundamentals, Phys. Rev. B **55**, 4275 (1997).

[10] A. M. Pendás, A. Costales, and V. Luaña, Ions in crystals: The topology of the electron density in ionic materials. III. Geometry and ionic radii, J. Phys. Chem. B **102**, 6937 (1998).

[11] G. V. Gibbs, M. B. Boisen, F. C. Hill, O. Tamada, and R. T. Downs, SiO and GeO bonded interactions as inferred from the bond critical point properties of electron density distributions, Phys. Chem. Minerals **25**, 574 (1998).

[12] G. V. Gibbs, K. M. Rosso, D. M. Teter, M. B. Boisen, Jr., and M. S. T. Bukowinski, Model structures and properties of the electron density distribution for low quartz at pressure: A study of the SiO bond, J. Mol. Struct. **485–486**, 13 (1999).

[13] G. V. Gibbs, R. Downs, D. F. Cox, K. M. Rosso, N. L. Ross, A. Kirfel, T. Lippmann, W. Morgenroth, and T. D. Crawford, Experimental bond critical point and local energy density properties determined for Mn–O, Fe–O, and Co–O bonded interactions for tephroite, Mn_2SiO_4, fayalite, Fe_2SiO_4, and Co_2SiO_4 olivine and selected organic metal complexes: Comparison with properties calculated for non-transition and transition metal M-O bonded interactions for silicates and oxides, J. Phys. Chem. A **112**, 8811 (2008).

[14] B. Dorado, M. Freyss, and G. Martin, GGA + U study of the incorporation of iodine in uranium dioxide, Eur. Phys. J. B **69**, 203 (2009).

[15] H. Y. Geng, Y. Chen, Y. Kaneta, M. Iwasawa, T. Ohnuma, and M. Kinoshita, Point defects and clustering in uranium dioxide by LSDA + U calculations, Phys. Rev. B **77**, 104120 (2008).

[16] T. Hartman, A. Alaniz, F. Poineau, P. F. Weck, J. A. Valdez, M. Tang, G. D. Jarvinen, K. R. Czerwinski, and K. E. Sickafus, Structure studies on lanthanide technetium pyrochlores as prospective host phases to immobilize ^{99}technetium and fission lanthanides from effluents of reprocessed used nuclear fuels, J. Nucl. Mater. **411**, 60 (2011).

[17] M. T. Weller, P. G. Dickens, and D. J. Penny, The structure of δ-UO_3, Polyhedron **7**, 243 (1988).

[18] E. H. P. Cordfunke and P. Aling, System $UO_3 + U_3O_8$: Dissociation pressure of γ-UO_3, Trans. Faraday Soc. **61**, 50 (1965).

[19] S. Siegel and H. R. Hoekstra, Bond lengths in gamma-uranium trioxide, Inorg. Nucl. Chem. Lett. **7**, 455 (1971).

[20] Y. Hinatsu, N. Masaki, and T. Fujino, The crystal structure of La_6UO_{12}, J. Solid State Chem. **73**, 567 (1988).

[21] J. P. Perdew, J. Chevary, S. Vosko, K. A. Jackson, M. R. Pederson, D. Singh, and C. Fiolhais, Atoms, molecules, solids, and surfaces: Applications of the generalized gradient approximation for exchange and correlation, Phys. Rev. B **48**, 4978(E) (1993).

[22] P. E. Blöchl, Projector augmented-wave method, Phys. Rev. B **50**, 17953 (1994).

[23] G. Kresse and J. Furthmüller, Efficiency of ab-initio total energy calculations for metals and semiconductors using a plane-wave basis set, Comput. Mat. Sci. **6**, 15 (1996).

[24] G. Kresse and J. Hafner, *Ab initio* molecular dynamics for liquid metals, Phys. Rev. B **47**, 558 (1993).

[25] S. L. Dudarev, D. N. Manh, and A. P. Sutton, Effect of Mott-Hubbard correlations on the electronic structure and structural stability of uranium dioxide, Philos. Mag. B **75**, 613 (1997).

[26] S. L. Dudarev, G. A. Botton, S. Y. Savrasov, C. J. Humphreys, and A. P. Sutton, Electron-energy-loss spectra and the structural stability of nickel oxide: An LSDA + U study, Phys. Rev. B **57**, 1505 (1998).

[27] N. A. Brincat, S. C. Parker, M. Molinari, G. C. Allen, and M. T. Storr, Ab initio investigation of the UO_3 polymorphs: Structural properties and thermodynamic stability, Inorg. Chem. **53**, 12253 (2014).

[28] H. He, D. A. Andersson, D. D. Allred, and K. D. Rector, Determination of the insulation gap of uranium oxides by spectroscopic ellipsometry and density functional theory, J. Phys. Chem. C **117**, 16540 (2013).

[29] D. Vega and D. Almeida, AIM-UC: An application for QTAIM analysis, J. Comput. Methods Sci. Eng. **14**, 131 (2014).

[30] G. Henkelman, A. Arnaldsson, and H. Jónsson, A fast and robust algorithm for Bader decomposition of charge density, Comput. Mater. Sci. **36**, 354 (2006).

[31] H. Y. Geng, H. X. Song, K. Jin, S. Xiang, and Q. Wu, First-principles study on oxidation effects in uranium oxides and high-pressure high-temperature behavior of point defects in uranium dioxide, Phys. Rev. B **84**, 174115 (2011).

[32] C. J. Pickard, B. Winkler, R. K. Chen, M. Payne, M. Lee, J. Lin, J. White, V. Milman, and D. Vanderbilt, Structural Properties of Lanthanide and Actinide Compounds within the Plane Wave Pseudopotential Approach, Phys. Rev. Lett. **85**, 5122 (2000).

[33] R. Shannon, Revised effective ionic radii and systematic studies of interatomic distances in halides and chalcogenides, Acta Crystallogr. Sect. A **32**, 751 (1976).

[34] R. Sanderson, *Chemical Bonds and Bonds Energy* (Elsevier, London, 2012).

[35] D. Gryaznov, E. Heifets, and E. Kotomin, *Ab initio* DFT + U study of He atom incorporation into UO_2 crystals, Phys. Chem. Chem. Phys. **11**, 7241 (2009).

[36] R. F. Bader and H. Essén, The characterization of atomic interactions, J. Chem. Phys. **80**, 1943 (1984).

[37] W. Zachariasen, Bond lengths in oxygen and halogen compounds of d and f elements, J. Less Common Met. **62**, 1 (1978).

[38] W. Zachariasen, Crystal chemical studies of the 5f-series of elements. XXIII. On the crystal chemistry of uranyl compounds

and of related compounds of transuranic elements, Acta Crystallogr. **7**, 795 (1954).

[39] I. D. Brown and D. Altermatt, Bond-valence parameters obtained from a systematic analysis of the inorganic crystal structure database, Acta Crystallogr. Sect. B **41**, 244 (1985).

[40] G. V. Gibbs, F. C. Hill, M. B. Boisen, and R. T. Downs, Power law relationships between bond length, bond strength and electron density distributions, Phys. Chem. Mineral. **25**, 585 (1998).

[41] G. V. Gibbs, M. B. Boisen, L. L. Beverly, and K. M. Rosso, A computational quantum chemical study of the bonded interactions in earth materials and structurally and chemically related molecules, Rev. Mineral. Geochem **42**, 345 (2001).

[42] L. Pauling, The principles determining the structure of complex ionic crystals, J. Am. Chem. Soc. **51**, 1010 (1929).

[43] D. Altermatt and I. D. Brown, The automatic searching for chemical bonds in inorganic crystal structures, Acta Crystallogr. Sect. B **41**, 240 (1985).

[44] H. Idriss, Surface reactions of uranium oxide powder, thin films and single crystals, Surf. Sci. Rep. **65**, 67 (2010).

[45] See Supplemental Material at http://link.aps.org/supplemental/10.1103/PhysRevMaterials.1.065404 for Fig. SM.1.1.

[46] See Supplemental Material at http://link.aps.org/supplemental/10.1103/PhysRevMaterials.1.065404 for Fig. SM.1.2.